Time-Dependent FEM Modeling for Transcutaneous Oxygen Sensors

Mohammed Almatrood[1] and Bige D. Unluturk[2]

***Abstract*— Continuous, real-time respiratory monitoring is essential in managing chronic respiratory diseases, perioperative care, and critical care settings, where the rapid and accurate detection of hypoxia can significantly impact patients' outcomes. Transcutaneous oxygen monitoring ($PtcO_2$) is an emerging wearable sensing technology that measures the partial pressure of oxygen diffusing through the skin which correlates with arterial oxygen partial pressure (PaO_2), the clinical gold standard. Despite its promise, the clinical adoption of $PtcO_2$ has been limited. Prior studies have primarily focused on direct comparisons between PaO_2 and $PtcO_2$, yielding mixed results regarding their agreement and limiting $PtcO_2$ to trend monitoring. To address this gap, we propose a finite element modeling (FEM) framework to investigate the physiological relationship between PaO_2 and $PtcO_2$. By simulating oxygen transport across multiple skin layers, the model provides mechanistic insights into transcutaneous oxygen dynamics under varying physiological conditions, such as arterial oxygen fluctuations and localized blood flow occlusion. This personalized computational model aims to improve the accuracy and reliability of transcutaneous oxygen monitoring, enabling more effective continuous respiratory assessment.**

I. INTRODUCTION

Accurate, real-time quantification of arterial oxygen partial pressure (PaO_2) is essential for effective management of various respiratory disorders, including chronic obstructive pulmonary disease (COPD) and asthma, among others. Clinical methods such as arterial blood gas analysis (ABG) and pulse oximetry are commonly used; however, both methods present significant limitations. For instance, ABG, while providing detailed and accurate insights into blood gas content, remains invasive, painful, and impractical for continuous monitoring, as it provides only a snapshot of a rapidly changing parameter [1]. Noninvasive method of pulse oximetry is widely used, but it measures only oxygen saturation (SpO_2) and is influenced by peripheral perfusion, ambient light conditions, skin pigmentation, leading to potential inaccuracies [2], [3].

Transcutaneous oxygen partial pressure ($PtcO_2$) monitoring is a promising method for continuous, non-invasive, real-time assessment. Luminescence-based wearable sensors have recently emerged as cost-effective tools for $PtcO_2$ measurement [4]. However, these devices face challenges stemming from physiological variability, which limits the reliability of $PtcO_2$ as a surrogate of PaO_2 [5], [6].

To overcome these limitations, this paper proposes a computational framework based on finite element modeling (FEM). We develop a 3D multilayer skin model and simulate the transport of oxygen through it. We incorporate adjustable parameters, such as skin thickness and oxygen consumption, to reflect individual variability, enabling more accurate and personalized transcutaneous oxygen monitoring.

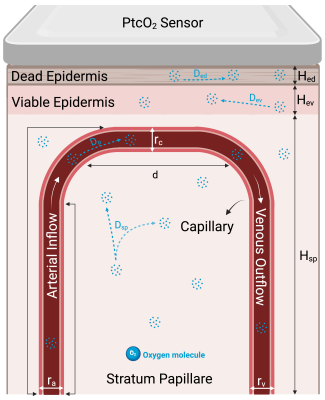

Fig. 1: Cross-section of skin microcirculatory unit [7].

II. RELATED WORK

Commercial transcutaneous oxygen monitoring devices use heating to enhance oxygen diffusion through the skin, considering that this allows $PtcO_2$ to approximate PaO_2. However, excessive heating can alter the local blood flow and cause vascular changes that may not reflect systemic oxygenation [8], while insufficient heating can lead to underestimation of tissue oxygen levels [9]. Heating also poses risks of skin burns and irritation, particularly in sensitive populations like neonates [10].

To address these limitations, a new luminescence-based transcutaneous sensing technology was developed that eliminates the use of heating elements [11]. However, this approach can potentially widen the discrepancy between PaO_2 and $PtcO_2$. To estimate PaO_2 from $PtcO_2$ even for the non-heating sensors, we aim to develop a model describing the relationship of $PtcO_2$ and PaO_2.

Oxygen transport in skin was first modeled by Krogh whose model describes radial oxygen diffusion from a capillary into surrounding tissue, assuming steady-state conditions and uniform consumption [12]. While foundational, it oversimplifies skin structure. Another approach by Grossman built a model based on multilayered skin structure and accounting for differences in diffusion coefficients and metabolic activity across layers [13].

III. METHODS

To investigate the relationship between $PtcO_2$ and PaO_2, we developed a partial differential equation (PDE)-based

[1]Mohammed Almatrood is with the Institute for Quantitative Health Science and Engineering, Department of Biomedical Engineering, Michigan State University, East Lansing, MI, USA, almatro2@msu.edu

[2]Bige D. Unluturk is with the Institute for Quantitative Health Science and Engineering, Departments of Electrical & Computer Engineering, and Biomedical Engineering, Michigan State University, East Lansing, MI, USA, unluturk@msu.edu

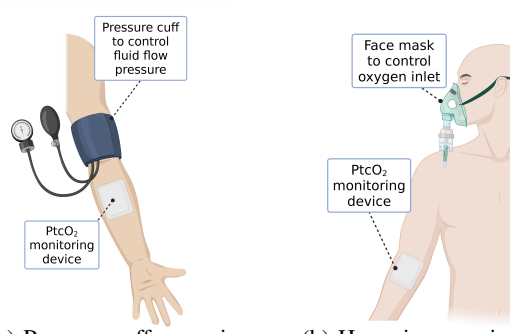

(a) Pressure cuff scenario. (b) Hypoxia scenario.

Fig. 2: Human tests scenarios used in FEM studies [14].

oxygen transport model within a 3D multilayer skin structure inspired by Grossmann's model (Fig. 1). FEM was then performed in COMSOL Multiphysics to simulate oxygen transport based on this model. We focused on time-dependent behavior to replicate the experimental conditions in [11], where $PtcO_2$ is measured under modulated PaO_2 using either local occlusion with blood pressure cuff or systemic hypoxia via hypoxia mask as shown in Fig. 2.

A. Grossmann's Model

The model describes oxygen dynamics within each layer:

- **Dead epidermis (ed, outer non-viable part of skin):** Oxygen transport is governed solely by diffusion, with no metabolic oxygen consumption.
- **Viable epidermis (ev, inner metabolically active region):** Transport of oxygen is diffusive, but with a constant rate of oxygen consumption.
- **Stratum papillare (sp, vascularized dermal layer beneath the epidermis):** This layer contains capillaries, and oxygen transport occurs via both diffusion and convection. Diffusion-driven transport with steady oxygen consumption is assumed within the surrounding tissue.

1) Oxygen Transport Equations: A set of PDEs was used to describe the blood flow and oxygen transport inside the capillaries and across each skin layer as follows

- Capillary (c) (diffusion and convection):

$$0 = \nabla \cdot (\alpha_c D_c \nabla P - V\,[\alpha_c P + H C_{Hb} S_0(P)]) \quad (1)$$

- Viable epidermis (ev) and stratum papillare (sp) (diffusion with consumption):

$$0 = \nabla \cdot (\alpha_i D_i \nabla P) - A(P), \quad i = \text{sp, ev} \quad (2)$$

- Dead epidermis (ed) (diffusion only):

$$0 = \nabla \cdot (\alpha_{ed} D_{ed} \nabla P) \quad (3)$$

Here, P denotes the oxygen partial pressure (kPa), α is the oxygen solubility coefficient (ml O_2/g-kPa), V is the velocity field (cm/s), C_{Hb} is the hemoglobin concentration (gHb/gblood), H is the Hüfner number (ml O_2/gHb), and $S_0(P)$ represents the oxygen-hemoglobin dissociation curve.

The oxygen dissociation curve is defined as

$$S_0(P) = \frac{1}{4} \sum_{i=1}^{4} \frac{i \cdot a_i \cdot P^i}{1 + \sum_{i=1}^{4} a_i \cdot P^i} \quad (4)$$

where a_i are the dissociation constants.

2) Fluid Flow Equations: The laminar flow of blood within the capillary is modeled using the incompressible Navier-Stokes equations

$$\rho \frac{\partial \mathbf{u}}{\partial t} + \rho(\mathbf{u} \cdot \nabla)\mathbf{u} = \nabla \cdot [-P \cdot \mathbf{I} + \mathbf{K}] + \mathbf{F}, \; \mathbf{K} = \mu(\nabla \mathbf{u} + (\nabla \mathbf{u})^T) \quad (5)$$

where ρ is the fluid density (kg/m^3), μ is the dynamic viscosity (Pa·s), $\mathbf{F}$ is the body force (N/m^3), and $\mathbf{I}$ is the identity matrix.

3) Boundary Conditions: The only boundary conditions considered at the skin surface were no-flux, assuming the sensor lies on top of the skin unit perfectly adhered, and effectively blocking oxygen exchange with the air, which can be expressed as $\frac{\partial P}{\partial n} = 0$ [13]. Sensing film thickness was assumed negligible.

4) Model Assumptions: Incompressible flow, i.e. $\nabla \cdot \mathbf{u} = 0$, and a no-slip boundary conditions were assumed at vessel walls, i.e. $\mathbf{u} = 0$, with initial conditions $\mathbf{u}_0 = \langle 0, 0, 0 \rangle$ m/s and $P_0 = 13.1$ kPa. A no-flux condition is applied at the outer lateral boundaries of the microcirculatory unit since oxygen flux across unit boundaries is considered negligible [13]. The reaction term for oxygen within the capillary is defined as $R_c = \nabla V \cdot (H\, C_{Hb}\, S_0(P))$, and at Sp and Ev the oxygen consumption, that is, $R_{sp} = R_{ev} = A = 2.23 \times 10^{-3}$ mol$/(m^3 \cdot s)$, with initial concentration $C_0 = 13.3$ kPa [13].

B. FEM Simulation

In experiments reported in [11], the transcutaneous sensor was tested by modulating PaO_2 via i) local occlusion restricting the blood flow and ii) systemic hypoxia reducing the overall oxygen intake as shown in Fig. 2.

We implemented our model in Section III-A using COMSOL Multiphysics. The Grossmann's microcirculatory model was geometrically constructed using a 3D representation with dimensions of 140 × 140 × 240 μm and incorporated a central capillary loop measuring 190 μm in height. Oxygenated blood enters from the arterial end and exits through the venous end of the capillary, with oxygen dissociating from hemoglobin and diffusing across the capillary walls into the surrounding skin layers as shown in Fig. 1.

The simulation utilized the *Laminar Flow* module to describe hemodynamics within the capillary loop, and the *Transport of Diluted Species* module to model oxygen transport across the skin and into the sensor layer. As COMSOL's transport modules require concentration as the dependent variable, Henry's Law was applied to convert oxygen partial pressure, P, to concentration, C, using the solubility coefficient, α, as $\alpha P = C$.

Within the *Laminar Flow* module, the capillary was modeled with a no-slip boundary condition and incompressible flow with backflow suppression. In the *Transport of Diluted Species* module, individual transport properties were assigned to each unit component (capillary, stratum papillare (sp), viable epidermis (ev), and dead epidermis (ed)) according to Eqs 1, 3, 2. Reaction boundary conditions were applied inside the capillary to account for hemoglobin-oxygen dissociation, and in the sp and ev layers for tissue

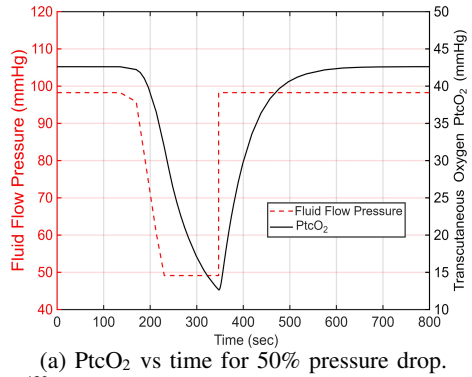

(a) $PtcO_2$ vs time for 50% pressure drop.

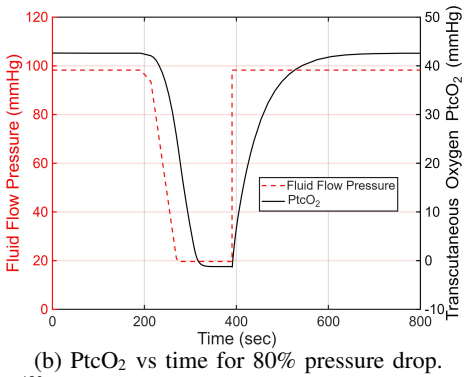

(b) $PtcO_2$ vs time for 80% pressure drop.

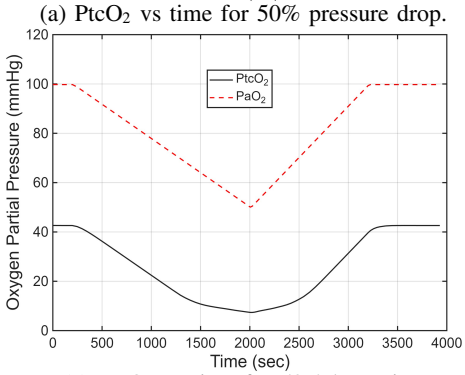

(c) $PtcO_2$ vs time for 50% hypoxia.

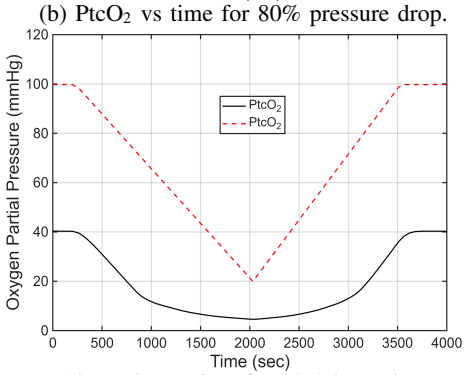

(d) $PtcO_2$ vs time for 80% hypoxia.

Fig. 3: Simulation results showing $PtcO_2$ with respect to time for local occlusion (a-b) and systemic hypoxia (c-d).

oxygen consumption. No-flux boundaries were enforced at all external surfaces. Once all governing equations and boundary conditions were established, the model was solved using the transient solver.

IV. Results and Discussion

The FEM study was divided into two parts: i) local blood flow occlusion and ii) systemic oxygen inflow variation.

A. Blood Flow Occlusion

As shown in Fig. 2a, applying a blood pressure cuff to upper arm restricts blood flow to the forearm, where the sensor is attached, represented by a drop in the blood pressure. A time dependent study was performed with 50% and 80% linear blood pressure drop and resulting $PtcO_2$ profiles are plotted with respect to time in (Fig. 3a) and (Fig. 3b). After the settling period, a linear occlusion was applied to the blood flow inlet at the capillary for 3 min and then removed. The simulated occlusions showed an immediate response in $PtcO_2$ levels, reflecting rapid physiological response to decreased perfusion. Notably, the more severe occlusion scenario with 80% pressure drop exhibited a lower $PtcO_2$ during occlusion and reaches this minimum faster, suggesting accelerated skin oxygen consumption due to limited oxygen availability. Post-occlusion recovery times (around 6 minutes) were consistent across scenarios, emphasizing delayed vascular and metabolic compensatory mechanisms. Unfortunately, there are no reported human data using non-heating $PtcO_2$ measurements for comparison. Moreover, comparison with current $PtcO_2$ devices, with heating elements, is invalid as their measurement will be closer to PaO_2 than our results. However, our recovery time and $PtcO_2$ behavior closely aligned with the experimental results reported in [11].

B. Oxygen Inflow Variation

To replicate the hypoxia study [11], a transient simulation was performed using two linear reductions in PaO_2, 50% (Fig. 3c) and 80% (Fig. 3d), modeled by a decrease in oxygen inflow at the arterial end of the capillary. Following a stabilization period, the oxygen drop was applied for 30 min and was allowed 20-25 min restoration period, based on the hypoxia level, according to [15]. The simulations showed a rapid initial decline in $PtcO_2$ under severe hypoxia, whereas moderate hypoxia resulted in a slower and more gradual decrease, indicating a delayed skin response to less drastic oxygen deprivation. The $PtcO_2$ levels gradually returned back to normal following the restoration trend.

Skin and oxygen transport properties vary across individuals due to a range of physiological and environmental factors, leading to differences in $PtcO_2$ measurements. To evaluate the impact of this variability, we adjusted model parameters based on literature for skin thicknesses [16] and oxygen diffusion coefficients [17]. The simulation results for $PtcO_2$ are shown with respect to time in Fig. 4a and Fig. 4b for different skin thickness factors, k, and in Fig. 4c and Fig. 4d for oxygen diffusion coefficient for both occlusion and hypoxia cases. Increasing skin thickness led to lower $PtcO_2$, which can account for personal variabilities in $PtcO_2$ among men and women. On the other hand, the increase in the diffusion coefficient affected $PtcO_2$ less, but it can be used to account for plasma composition due to illnesses.

V. Conclusion

Our FEM model accurately simulates the dynamic physiological responses of $PtcO_2$ to both local and systemic changes in PaO_2, demonstrating trends consistent with human experimental data. We also introduce a method for cap-

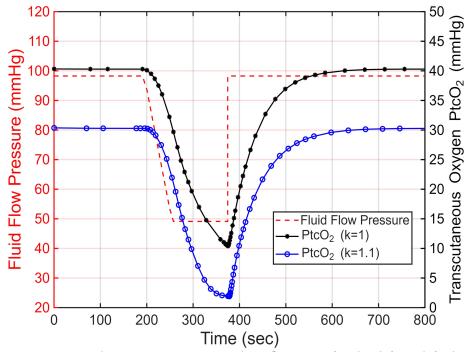

(a) Pressure drop FEM results for varied skin thickness.

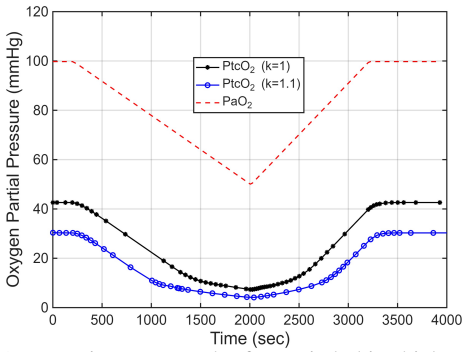

(b) Hypoxia FEM results for varied skin thickness.

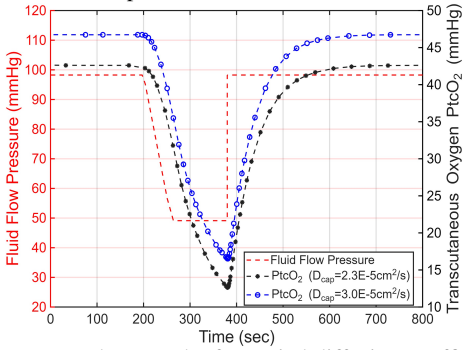

(c) Pressure drop results for varied diffusion coefficient

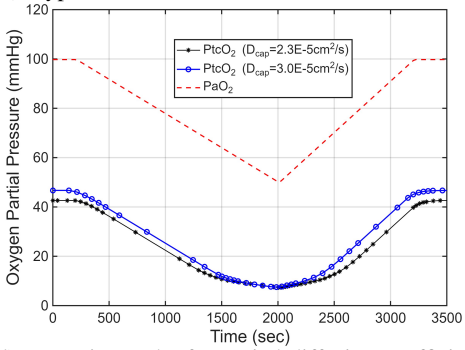

(d) Hypoxia results for varied diffusion coefficient.

Fig. 4: $PtcO_2$ for varying skin thickness (a-b) and diffusion coefficient (c-d) for occlusion (a-c) and hypoxia (c-d).

turing inter-individual variability by adjusting model parameters to reflect personal physiological differences. While still in development, this modeling framework lays the foundation for estimating PaO_2 from $PtcO_2$ measurements combined with personal parameters. This advancement significantly enhances the clinical utility of transcutaneous oxygen sensors and highlights their potential in personalized wearable devices for reliable, continuous respiratory monitoring.

VI. Acknowledgment

This material is based upon work supported by the National Science Foundation under Grant No. OAC-2203827, and by National Institute of Health under Grant No. R01HL172293 and No. R21EB036329. We also thank our collaborator Dr. Ulkuhan Guler and her team in WPI.

References

[1] J. H. Storre, F. S. Magnet, M. Dreher, and W. Windisch, "Transcutaneous monitoring as a replacement for arterial pco2 monitoring during nocturnal non-invasive ventilation," *Respiratory medicine*, vol. 105, no. 1, pp. 143–150, 2011.

[2] A. Fawzy, T. D. Wu, K. Wang, M. L. Robinson, J. Farha, A. Bradke, S. H. Golden, Y. Xu, and B. T. Garibaldi, "Racial and ethnic discrepancy in pulse oximetry and delayed identification of treatment eligibility among patients with covid-19," *JAMA internal medicine*, vol. 182, no. 7, pp. 730–738, 2022.

[3] W. Van Weteringen, T. G. Goos, T. Van Essen, C. Ellenberger, J. Hayoz, R. C. De Jonge, I. K. Reiss, and P. M. Schumacher, "Novel transcutaneous sensor combining optical tcpo 2 and electrochemical tcpco 2 monitoring with reflectance pulse oximetry," *Medical & Biological Engineering & Computing*, vol. 58, pp. 239–247, 2020.

[4] I. Costanzo, D. Sen, J. Adegite, P. M. Rao, and U. Guler, "A noninvasive miniaturized transcutaneous oxygen monitor," *IEEE Transactions on Biomedical Circuits and Systems*, vol. 15, no. 3, pp. 474–485, 2021.

[5] M. M. Kmieć, H. Hou, M. L. Kuppusamy, T. Drews, A. M. Prabhat, S. Petryakov, E. Demidenko, P. E. Schaner, J. C. Buckey, A. Blank, and P. Kuppusamy, "Transcutaneous oxygen measurement in humans using a paramagnetic skin adhesive film," *Magnetic Resonance in Medicine*, vol. 81, pp. 781–794, 2018.

[6] T. Essen, N. Gangaram-Panday, W. Weteringen, T. Goos, I. Reiss, and R. Jonge, "Improving the clinical interpretation of transcutaneous carbon dioxide and oxygen measurements in the neonatal intensive care unit," *Neonatology*, vol. 120, pp. 308–316, 2023.

[7] M. Almatrood, "Grossmann's cross sectional model," https://BioRender.com/k1g5oj9, 2025, created in BioRender.

[8] P. Pape, Z. M. Piosik, C. M. Kristensen, J. Dirks, L. S. Rasmussen, and M. S. Kristensen, "Transcutaneous carbon dioxide monitoring during prolonged apnoea with high-flow nasal oxygen," *Acta Anaesthesiologica Scandinavica*, vol. 67, pp. 649–654, 2023.

[9] A. Cheung, L. Tu, A. Macnab, B. K. Kwon, and B. Shadgan, "Detection of hypoxia by near-infrared spectroscopy and pulse oximetry: a comparative study," *Journal of Biomedical Optics*, vol. 27, 2022.

[10] A. Conway, E. Tipton, W. Liu, Z. J. Conway, K. Soalheira, J. Sutherland, and J. Fingleton, "Accuracy and precision of transcutaneous carbon dioxide monitoring: a systematic review and meta-analysis," *Thorax*, vol. 74, pp. 157–163, 2018.

[11] V. Vakhter, B. Kahraman, G. Bu, F. Foroozan, and U. Guler, "A prototype wearable device for noninvasive monitoring of transcutaneous oxygen," *IEEE Transactions on Biomedical Circuits and Systems*, vol. 17, no. 2, pp. 323–335, 2023.

[12] A. Krogh, "The number and distribution of capillaries in muscles with calculations of the oxygen pressure head necessary for supplying the tissue," *The Journal of physiology*, vol. 52, no. 6, p. 409, 1919.

[13] U. Grossmann, "Simulation of combined transfer of oxygen and heat through the skin using a capillary-loop model," *Mathematical Biosciences*, vol. 61, no. 2, pp. 205–236, 1982.

[14] M. Almatrood, "Human tests scenarios setups," https://BioRender.com/w7zam3o, 2025, created in BioRender.

[15] M. S. Rahman and P. Thomas, "Molecular and biochemical responses of hypoxia exposure in atlantic croaker collected from hypoxic regions in the northern gulf of mexico," *PLoS One*, vol. 12, no. 9, p. e0184341, 2017.

[16] J. Derraik, M. Rademaker, W. Cutfield, T. Pinto, S. Tregurtha, A. Faherty, J. Peart, P. Drury, and P. Hofman, "Effects of age, gender, bmi, and anatomical site on skin thickness in children and adults with diabetes," *Plos One*, vol. 9, p. e86637, 2014.

[17] N. Patel and K. Patel, "Estimation of pulmonary gas exchange in the human respiratory system under normal and abnormal conditions," *Biosciences Biotechnology Research Asia*, vol. 20, no. 1, pp. 255–262, 2023.